Supplementary information for Modal gain enhancement of perovskite nanosheets by a patterned waveguide via spectral-length gain analysis

Inhong Kim[1], Ga Eul Choi[1], Ming Mei[1], Minwoo Kim[1], Minju Kim[1], Young Woo Kwon[2], Tae-In Jeong[1], Seungchul Kim[1], Suck Won Hong[1], Kwangseuk Kyhm[1], and Robert A. Taylor[3]

[1]Department of Opto & Cogno Mechatronics Engineering, RCDAMP, Pusan National University, Busan 46241, Republic of Korea
[2]Department of Nano-Funsion Technology, Pusan National University, Busan 46241, Republic of Korea
[3]Clarendon Laboratory, Department of Physics, University of Oxford, Oxford, OX1 3PU, U.K

Patterned PUA waveguide fabrication

In order to prepare the PDMS mold, a drop of photoresist was placed on a chrome-coated glass substrate ($100 \times 100 \times 0.5$ mm), a spin-coating process was performed at a spin speed of 750 rpm for 30 s. The coated substrate was then soft-baked at a temperature of 110°C for 10 minutes. The substrate was then placed under a patterned mask and illuminated by UV radiation at 1800 mJ/cm^2, the substrate and PR developing process took 20 min using developer solution. After rinsing with deionized water, the patterned mold was completely dried on a hot plate. To fabricate a PDMS replica, PDMS prepolymer with curing agent solution was poured on the patterned mold and cured at 80°C for 1 h. Subsequently, an appropriate amount of PUA resin was dropped on the PDMS mold to create a line-patterned substrate. Then, PET guide film was located on the PUA resin and rolled using a roller for conformal contact between the PUA resin and the PET film. The PUA resin was then exposed to UV light at $\lambda = 365$ nm. After curing completely, the PDMS mold was carefully detached from the patterned PUA substrate. Figure S1 shows the sequential molding process used to prepare a PUA substrate via nano-imprint lithography.

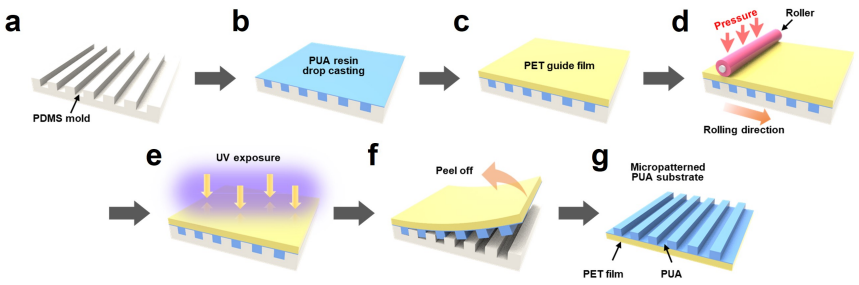

Figure S1: Schematic illustration of the sequential molding process to prepare a PUA substrate via nano-imprint lithography. **a** The PDMS master mold is prepared by conventional lithography (SU-8). **b** PUA resin was cast by a spin coating process. **c** A PET backing guide film was contacted on top of the PUA resin. **d** A roller was used with mild pressure to form a conformal wetting between the PET backing and the PUA resin. **e** UV exposure (365 nm) was applied through the PET film (i.e., step-and-flash imprint lithography). **f-g** peeling off the patterned PUA/PET film.

Capillary-directed self-assembly of perovskite nanosheets

The line-patterned PUA substrate ($2 \times 2\,\mathrm{cm}^2$) was used without any additional cleaning process. The deposition process for the $CsPbBr_3$ nanosheets on the line-patterned substrate was conducted on a hot plate set at 60°C to facilitate the evaporation of the solvent (hexane) and the deposition. Next, the upper blade was installed at a 30°angle, and the colloidal perovskite solution was injected in a confined geometry containing the upper blade and the lower substrate. The trapped meniscus was formed by capillary force in this restricted geometry, and 20 cycles of one-way motion were performed at a speed of 2.5 mm/s by a computer-controlled translation stage. A uniformly stacked perovskite nanosheet film layer on PUA microfluidic channels was obtained through this repetitive capillary-directed self-assembly process. After the deposition process, the multi-stacked perovskite nanosheets on a patterned substrate were stored in a vacuum desiccator for further measurement and experiments. Figure S2 show an SEM image of the uniformly stacked $CsPbBr_3$ nanosheets on a line-patterned PUA substrate, which is fabricated by capillary directed self-assembly.

The thickness of the $CsPbBr_3$ nanosheets was measured using an AFM (Park systems, NX10). In Figure S3, an AFM image of $CsPbBr_3$ nanosheets on a SiO_2/Si substrate is shown, where the height and lateral profiles at selected areas were also obtained.

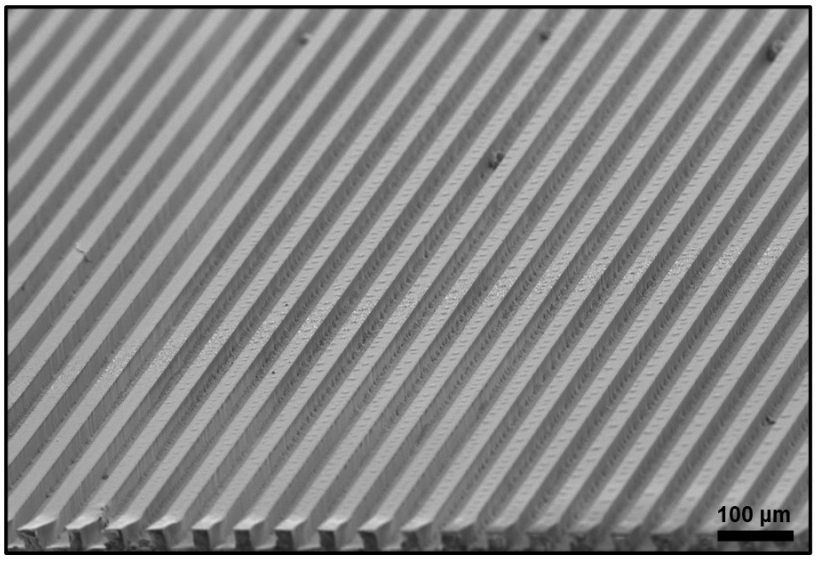

Figure S2: SEM image of uniformly stacked perovskite nanosheets on a line-patterned PUA substrate, which is fabricated by capillary-directed self-assembly.

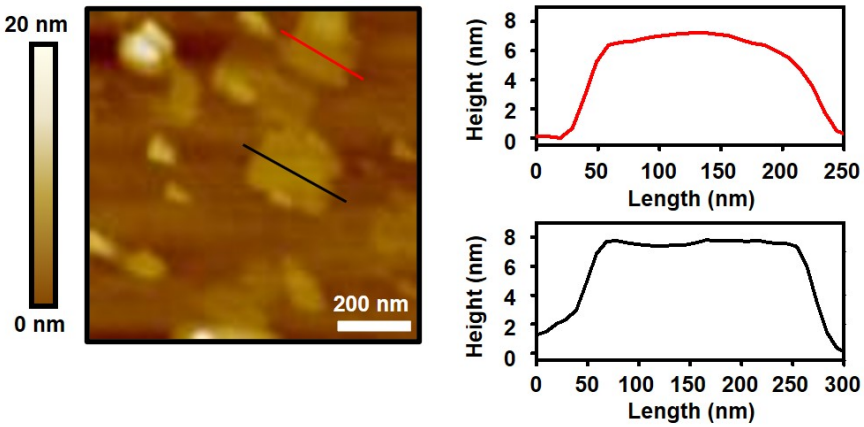

Figure S3: A typical AFM image of $CsPbBr_3$ nanosheets on a SiO_2/Si substrate (left), and the corresponding height profile for each location marked with red and black (right).

Variable stripe length method

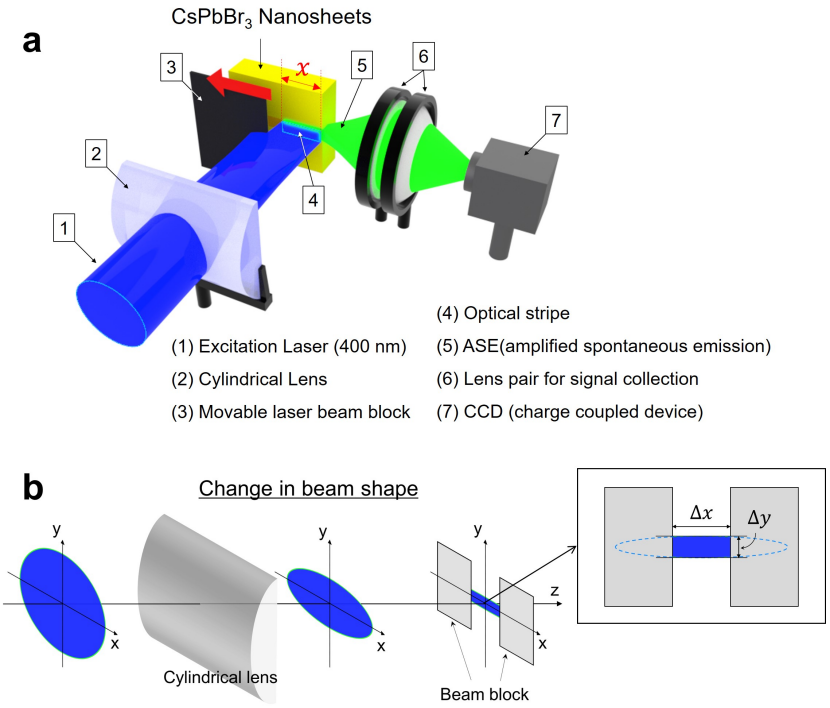

Figure S4: **a** A schematic of the vertical stripe length method (VSLM) setup. **b** A circular beam becomes a rectangular stripe by using a cylindrical lens.

The optical arrangement for the VSLM setup is shown schematically in Figure S4**a**. For excitation, 400 nm laser pulses (1) were used, which were obtained via second harmonic generation from fundamental laser pulses at 800 nm from a mode-locked Ti:Sapphire laser operating at 80 MHz repetition rate. The circular laser spot becomes a stripe shape after passing through a cylindrical lens (2), and is focused on the sample. The optical stripe length (x) was adjusted by a movable laser beam block (3) with a $\Delta x = 5\,\mu$m step size. Because of the Gaussian intensity distribution of a laser spot, an inhomogeneous intensity still remains along the optical stripe (4), and the stripe has a vertical width (Δx). The intensity distribution along the stripe can be measured by the knife-edge method or a beam profiling instrument, and the uniformity can also be enhanced by using a beam expander before the cylindrical lens. Within the measurement stripe length range, we have confirmed that the stripe beam intensity shows 20 % decrease over a whole stripe length $\sim 700\,\mu$m.

The edge emission spectrum (5) was collected by a lens pair (6), and detected by charge-coupled device (7). Because the sample is mounted in a cryostat, the

distance from the sample edge to the lens pair is far larger than the stripe length itself. Therefore, the solid angle can be assumed to be constant (i.e. $\Omega(x) \simeq \Omega$). Figure S4**b** shows how a circular laser beam becomes a rectangular stripe with an elliptical shape, where the length (Δx) and the width (Δy) of a rectangular stripe can be determined by a pair of beam blocks. The Δx is changed by a motorized moving beam block with a 5 μm step whilst the width remains constant $\Delta y \sim 50\,\mu$m.

Analysis of the stripe length-dependent ASE intensity

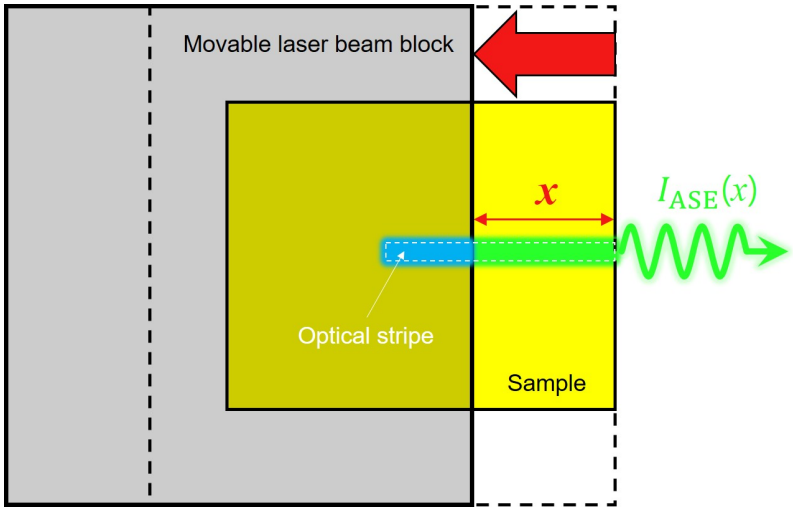

Figure S5: Schematic of one-dimensional amplification.

When an optical stripe length x is set by the movable beam block, the amplified spontaneous emission (ASE) at x can be collected from the open edge, where the ASE intensity $I(\hbar\omega, x)$ depends on both the energy ($\hbar\omega$) and stripe length (x). Additionally, spontaneous emission should be considered, which is given by $J_{\mathrm{sp}}\Omega$, where J_{sp} is the spontaneous emission density and Ω is the solid angle, respectively. Suppose the optical stripe is a one-dimensional amplifier, then the differential equation for $I(\hbar\omega, x)$ becomes:

$$\frac{\mathrm{d}I(\hbar\omega, x)}{\mathrm{d}x} = gI(\hbar\omega, x) + J_{\mathrm{sp}}(\hbar\omega)\Omega. \tag{1}$$

Suppose the modal gain coefficient $g(\hbar\omega)$ at a certain energy $\hbar\omega$ is constant, the solution to Eq. (1) is then:

$$I(\hbar\omega, x) = \frac{J_{\mathrm{sp}}(\hbar\omega)\Omega}{g(\hbar\omega)}(\mathrm{e}^{g(\hbar\omega)x} - 1). \tag{2}$$

To obtain a modal gain coefficient $g(\hbar\omega)$, Eq. (2) is compared with the stripe length dependent ASE intensity selected at a particular emission energy ($\hbar\omega$), where the two fitting parameters of $g(\hbar\omega)$ and $J_{\rm sp}(\hbar\omega)\Omega$ need to be optimized. However, unavoidable differences are always observed in the VSLM experiment. First, $I(\hbar\omega, x)$ shows a linearly increase when the stripe length x is less than a threshold value length $x_{\rm th}$ due to the finite stripe width. The stripe length needs to be longer than the stripe width of 50 μm. Second, an offset signal can be observed at the position of $x = 0$ due to laser diffraction. Therefore, Eq. (2) needs to be modified as:

$$I(x) = \frac{J_{\rm sp}\Omega}{g}\Big(\exp[g(x - x_{\rm th})] - 1\Big) + I_{\rm off}. \tag{3}$$

Furthermore, the empirical fitting of function of Eq.(3) is not a solution of Eq.(1), and $x_{\rm th}$ and $I_{\rm off}$ depend on experimental conditions. For example, $x_{\rm th}$ increases for a small gain medium. Even if the same medium is used, $x_{\rm th}$ also depends on the emission energy. In the case of strongly localized defect states, which which occurs at low spectral energy, $x_{\rm th}$ is relatively long. Third, an upper limit for the stripe length has to be selected, the so-called saturation length $x_{\rm sat}$ as $I(\hbar\omega, x)$ deviates gradually from exponential growth ($\sim {\rm e}^{g(\hbar\omega)x}$) near the saturation length $x_{\rm sat}$. Consequently, the fitting has to be done within a selected range of stripe lengths ($x_{\rm th} < x < x_{\rm sat}$). The saturation length $x_{\rm sat}$ is also determined with uncertainties, and the emission energy dependence is often ignored. Consequently, the current fitting method provides an average gain over a particular range ($x_{\rm th} < x < x_{\rm sat}$), but uncertainties are unavoidable in the gain magnitude and spectrum width.

As an alternative method, the gain can be obtained from the fundamental differential equation (1) as

$$g(\hbar\omega, x) = \frac{\frac{{\rm d}I(\hbar\omega,x)}{{\rm d}x} - J_{\rm sp}\Omega}{I(\hbar\omega, x)}. \tag{4}$$

For the first step, $\frac{{\rm d}I}{{\rm d}x}$ needs to be calculated from $I(x)$ at a selected $\hbar\omega$. For the second step, the constant linear slope near $x < x_{\rm th}$ is used for $J_{\rm sp}\Omega$. When the noise of $\frac{{\rm d}I}{{\rm d}x}$ is too large to define a constant slope, an average slope or the slope at a particular length can be used for consistency. For the third step, the numerator $\frac{{\rm d}I(\hbar\omega,x)}{{\rm d}x} - J_{\rm sp}\Omega$ is divided by the denominator $I(\hbar\omega, x)$. In this case, the small noise of $I(\hbar\omega, x)$ is likely to be amplified. Therefore, the offset near $x \simeq 0$ is useful in the last calculation, and noise filtering is necessary, otherwise the retrieved gain spectrum shows a small signal-to-noise ratio as the denominator noise becomes amplified. Nevertheless, the shape of gain spectrum is dominated by the derivative spectrum $\frac{{\rm d}I(\hbar\omega,x)}{{\rm d}x}$, and it is also useful to evaluate the degree of amplification. As a detail of the data calculation, the length differentiation to a data matrix $I(\hbar\omega, x)$ needs to be performed first at a selected $\hbar\omega$, and the derivative spectrum $\frac{{\rm d}I(\hbar\omega,x)}{{\rm d}x}$ can then be obtained by transposing the resultant matrix.

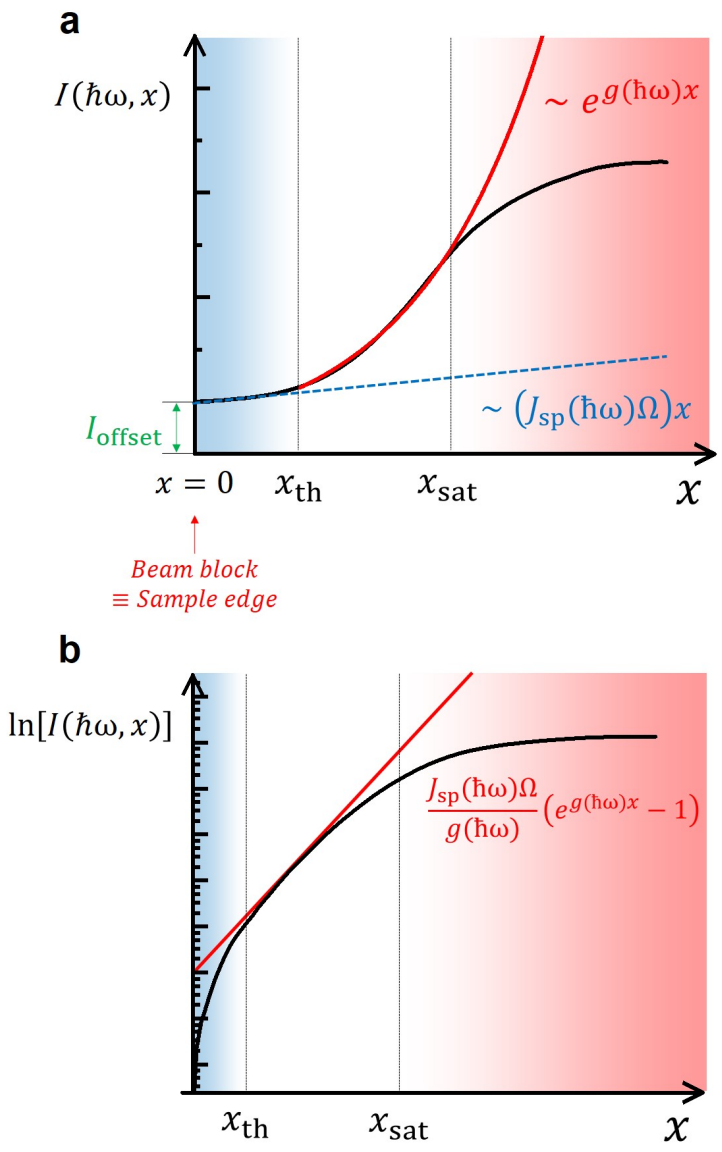

Figure S6: $I(\hbar\omega, x)$ and $J_{sp}(\hbar\omega)\Omega$ at **a** linear and **b** logarithmic scales.

Theoretical simulation for beam propagation within a waveguide

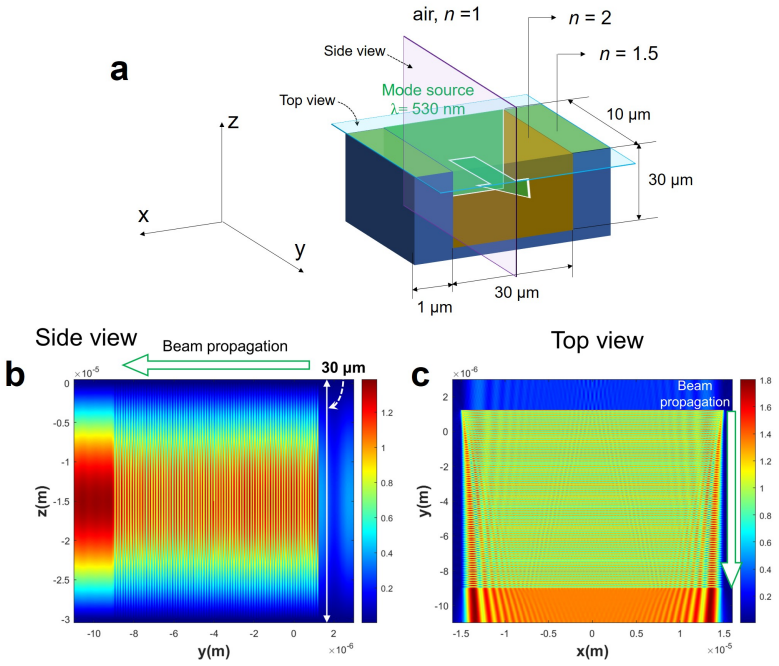

Figure S7: Theoretical simulation of beam propagation along the rectangular waveguide with 30 μm width and 30 μm height.

In order to confirm the mode confinement in an top-open waveguide structure, the waveguide propagation characteristics of the perovskite nanosheet layer were calculated by solving Maxwell's equations with a finite difference time-domain (FDTD) method. Figure S7.a illustrates the geometry of the perovskite nanosheet layer employed in the experiment. The core region (refractive index, $n = 2$) is set to be surrounded by a cladding region (refractive index, $n = 1.5$), while the top structure is open to free space (refractive index, $n = 1$). A perfectly matched layer (PML) was used as a boundary condition, which is impedance-matched to the surrounding material to prevent reflection errors. The wavelength of the mode source was set to 530 nm to match the peak wavelength of the amplified spontaneous emission (ASE). Figure S7.b and S7.c display the side and top-view cross-sections of the electric field profile propagating inside the waveguide, respectively.